Combined photoacoustic and photoconductive spectroscopic investigation of nonradiative recombination and electronic transport phenomena in crystalline *n*-type CdS. II. Theory

Edwin K. M. Siu and Andreas Mandelis
Photoacoustic and Photothermal Sciences Laboratory, Department of Mechanical Engineering, University of Toronto, Toronto, Ontario, Canada M5S 1A4
(Received 1 April 1986)

A theoretical model of the coupled photoconductive (PC) and microphone gas-coupled photoacoustic (PA) signal generation is presented. The model includes numerical solutions to the following: (i) the carrier transport equations leading to PC signal generation in the presence of two different types of recombination centers, (ii) the Poisson equation relating the difference between electron and hole densities to the internal electric field, and (iii) the heat diffusion equation, relating the carrier population density to the heat generation rate and ultimately to the PA signal generation. Spectroscopic simulations with the CdS absorption spectrum as input data essentially show agreement between theory and experiment in the band-gap and sub-band-gap spectral regions. Parameter variation reveals that PA and PC experimental data (preceding paper) can be predicted if, and only if, a wavelength-dependent nonradiative quantum efficiency is assumed with a substantial increase at photon energies below the band gap, coupled with signal contributions at higher photon energies due to band-to-band intrinsic transitions.

I. INTRODUCTION

The theory of the photoacoustic effect in solids developed by Rosencwaig and Gersho[1] (RG) has been the foundation for the development of specialized photoacoustic theories of semiconductors.[2–6] In the RG model the heat generation in a solid was assumed to occur instantaneously at the same spatial position where the exciting photons were absorbed. In semiconductors, light absorption is usually accompanied by energy migration before the transfer of the excited carrier energy to the lattice via nonradiative deexcitation transitions generating the photoacoustic (PA) signal source.[7] During their finite lifetime carriers in excited states can diffuse under population gradients[8] or drift under the influence of external electric fields[2,6] through finite distances in a crystal. As a result, the distribution of the optical energy in a semiconductor is not the same as that of the thermal energy. The spatial distributions of free electrons and holes in semiconductors depend upon the electronic properties of these materials, such as the surface recombination velocity and the diffusion coefficient of the carriers. Therefore, the PA signal is expected to contain information about these electronic parameters. The degree of usefulness of existing mathematical models must be judged in relation to the success of such models in incorporating and predicting PA signal dependence on these parameters. Among the available theories, Miranda[3] presented a one-dimensional model of the PA effect in semiconductors by taking into account carrier (electron and hole) diffusion and recombination. He solved the carrier diffusion equation for electrons and the heat diffusion equation and thus determined the PA response in terms of various semiconductor transport parameters. For instance, he was able to deduce the electronic lifetime and diffusion coefficient from the slope of the theoretical PA magnitude versus light modulation frequency response curve. The heat generation term, however, used in his work was

$$Q_s(x,t)=\left[\frac{\eta_{\text{nonrad}}\beta I_0}{h\nu}\right]\exp(\beta x)\exp(i\omega_0 t)\ , \tag{1.1}$$

where η_{nonrad} is the nonradiative quantum efficiency of the electron de-excitation process, $\beta(\nu)$ is the semiconductor absorption coefficient at optical frequency ν, I_0 is the irradiance of the incident light beam, and ω_0 is the angular frequency of light intensity modulation. Equation (1.1) is generally incomplete because it does not take into account carrier diffusion and recombination processes. Furthermore, the contribution of the surface recombination of free electrons and holes to the heat generation rate was also ignored. Sandomirskii *et al.*[4,5] used a similar theoretical approach to that of Miranda's, with the complete expression for the heat generation term. These authors focused their analysis on the modulation frequency dependence of the PA phase. They predicted the occurrence of phase peaks and valleys, which were theoretically related to thermal and electronic properties of the semiconductor, e.g., the thermal diffusivity, the ambipolar diffusion coefficient, and the lifetime of free carriers. These characteristic frequencies were found to be on the order of 10—70 kHz and, therefore, impractical for microphone gas-coupled experimental PA implementation. Vasil'ev and Sandomirskii[6] further presented a PA theory of semiconductors which were subjected to an alternating (AC) electric field. They deduced phase frequency dependences on the same thermal and electronic transport prop-

erties as those in Refs. 4 and 5 with similar experimental limitations. Bandeira *et al.*[2] used an approach somewhat different from those other workers by presenting a PA theory of semiconductors with an applied dc transverse electric field across the crystal, while taking electron diffusion effects into account. These authors assumed, however, no contributions to charge diffusion from holes, constant nonradiative quantum efficiencies throughout the optical-absorption spectrum of the semiconductor, and negligible trapping and/or recombination state densities. Their theory, nevertheless, showed considerable general agreement with experimental data from a CdS crystal of unknown origin and specifications, especially in the spectral range of photon energies higher than 2.4 eV (520 nm), which lie at or above the band-gap energy of this semiconductor.

The common shortfalls of all the existing PA theories when applied to pure CdS single crystals are (i) their inability to account for the presence of sub-band-gap trapping centers, which are known to exist in large densities in this semiconductor;[9,10] and (ii) their suitability to problems relevant only to extrinsic (impurity) semiconductors, whose transport properties are determined almost entirely by minority carrier statistics. In the case of pure CdS, and other II-VI compound semiconductors of this type, single crystals tend to be *n* type and, when properly self-compensated, to behave like high-resistivity intrinsic semiconductors. A rigorous determination of the photoacoustic and photoconductive signal source generation in intrinsic semiconductors involves the solution of three time-dependent simultaneous equations: two equations for the electron and hole transports, and Poisson's equation for space charge. The resulting carrier distributions can then be used directly to calculate the photocurrent density. They can further be used to calculate the crystal heat generation rate as a result of nonradiative recombinations. This rate will then be the thermal driving forcing function to the heat diffusion equation in the solid, which will ultimately generate the photoacoustic pressure pulse in the microphone chamber according to the RG model.[1]

In this work we have solved the above mentioned set of equations using the optical-absorption spectrum of CdS as an input excitation function which induces optical, electronic, and thermal responses in this material. The rigorous solution of the set of differential equations with no *a priori* simplifying assumptions requires a numerical approach, such as the finite difference method which we used in this paper. The use of a numerical method further allowed us to take into account the presence of sub-band-gap optical defect level mass-action statistics, without the requirement of detailed knowledge of the trapping mechanism at electron and hole-trapping centers. No assumption of a spatially linear relationship between electron and hole densities had to be made,[11] nor had the solutions to be confined to the steady state limit[12] as did previous analytical treatments of carrier transport equations. The solutions obtained numerically were applied to the experimental case of primary photoacoustic PA and photoconductive (PC) spectra acquisition in the presence of a transverse dc electric field across the crystal excited by modulated monochromatic illumination (See Paper I, Sec. III B).

II. ENERGETICS OF RECOMBINATION DEFECT CENTERS IN PURE CdS CRYSTAL

The nature and energy levels of defects responsible for the PA and PC spectroscopic behavior in the sub-band-gap region are of importance in estimating the contributions of mass-action statistics to the theoretical response of high-resistivity CdS single crystals. Such defects have been known to be responsible for radiative recombination and trapping of free carriers, resulting in orange luminescence[13–16] at low temperatures. Recently, orange luminescence was reported in low-resistivity CdS crystals at room temperature,[17] and was also visually observed[18] in high-resistivity CdS at room temperature. Some of the earlier investigations[14,15] on the possible origin of the luminescence resulted in contradicting models. The problem lay in the difficulty of identification of the origin of orange luminescence events, following either a band-to-defect level or a defect-to-defect level electronic transition. More recently, Mochizuki *et al.*[16] resolved that issue from the photoluminescence spectra of CdS_xSe_{1-x} and $Cd_yZn_{1-y}S$ solid solutions. From their results, the probable emission mechanism appeared to be a donor defect-to-acceptor defect level pair recombination with the donor level located 0.21 eV below the conduction band minimum, and the acceptor level at 0.29 eV above the valence band maximum of CdS at 4.2 K. The donor responsible for the emission seemed to be related to native defects, such as Cd interstitials or S vacancies. The nature of the acceptor defect center is unknown to date. Other authors have identified some of the energy levels associated with various defects in pure CdS. The main results are shown in Table I. Based on those findings, a partial picture of the energy levels of major defect centers in the band gap of pure CdS can be constructed as shown in Fig. 1. In that figure, energy bands, rather than levels, have been drawn for defects with more than one reported associated value in Table I. Taking the results by Mochizuki *et al.*[16] into account, and a value for our CdS crystal gap width $E_g \approx 2.56$ eV,[18] Fig. 1 shows that orange luminescence will cease if the photon energy of the optical excitation falls below the 2.31 eV level on the average. This approximate energy value is required to optically excite electrons from the filled band to defect levels of the doubly ionized sulphur vacancy. The photon energy of 2.31 eV corresponds to about 534 nm, which agrees closely with our visual observation[18] that orange luminescence ceased at wavelengths longer than approximately 525 nm. It thus appears likely that the observed PA and PC maxima[18] at around 529—530 nm are due to the cessation or orange luminescence and the rechanneling of the excitation energy to nonradiative recombinations with a corresponding increase in the nonradiative quantum yield η_{nonrad}. The above mechanism might be expected to break down, if there was active participation of the V_{Cd} defect which lies somewhat lower than the $V_{S^{2-}}$ defect band in Fig. 1. Therefore, it must be assumed that the V_{Cd} center cannot interact directly with the orange luminescence generation process in our crystals. The absence of any

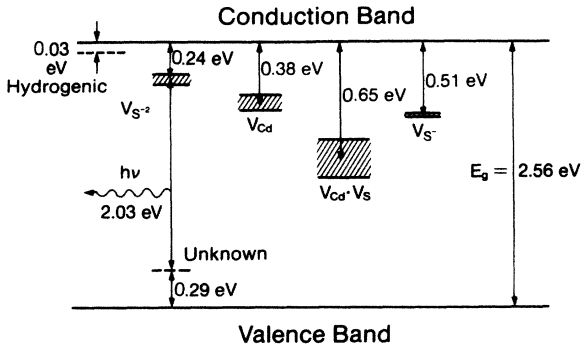

FIG. 1. Major defect species and energy level location in the bandgap of pure CdS. Energy bands are shown shaded where more than one value is cited in the literature (Table I), instead of single levels.

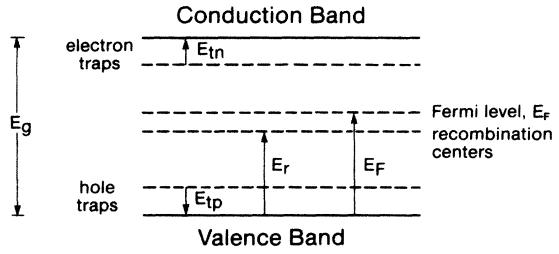

FIG. 2. Simplified CdS band-gap configuration adopted in the theory. E_{tn}: electron trap ionization energy; E_{tp}: hole trap ionization energy; E_r: recombination center activation energy.

measurable V_{Cd} concentration is also supported by Uchida's work,[10] who has concluded that vapor-grown pure CdS crystals with resistivity in the neighborhood of 10^6 Ω cm contained little or no cadmium vacancies. Uchida further showed that the PC maximum at around 529 nm disappeared after the deliberate formation of cadmium vacancies in the bulk of the crystal.

III. THEORY

In view of the discussion in Sec. II above, and for simplicity purposes, the theoretical model to be used consists of one type of electron trap, one type of hole trap, and one major recombination center in agreement with Bube's PC analysis.[19] As examples of defect centers acting as electron traps may be doubly ionized sulphur vacancies, $V_{S^{2-}}$, while deeper defects, such as Cd and S vacancy complexes, Fig. 1, may act as recombination centers. Defect levels close to the valence band edge may act as hole traps, such as the center of unknown origin identified by Mochizuki *et al.*[16] The simplified version of the CdS band-gap energetics used in the theory is shown in Fig. 2.

A. Carrier transport formalism

To describe the carrier distribution inside the crystal, the electron and hole transport equations must be solved,[11]

$$\frac{\partial}{\partial t}n(y,t)=G(y)-R(y,t)+\frac{\partial}{\partial y}\left[n(y,t)\mu_n E(y)+D_n\frac{\partial}{\partial y}n(y,t)\right], \quad (3.1)$$

$$\frac{\partial}{\partial t}p(y,t)=G(y)-R(y,t)-\frac{\partial}{\partial y}\left[p(y,t)\mu_p E(y)-D_p\frac{\partial}{\partial y}p(y,t)\right], \quad (3.2)$$

coupled with Poisson's equation,

TABLE I. Pure CdS defect species identification and position below the conduction-band minimum.

Possible defect	Temperature (°C)	E (eV)	Reference
$V_{S^{-2}}$	−170	0.20−0.21	(a)
	−135	0.25−0.30	(a)
	−150	0.24	(b)
V_{Cd}	−90	0.31−0.41	(a)
	−50	0.42−0.44	(a)
	−50	0.38	(b)
	−100	0.32	(b)
V_{S^-}	0	0.51−0.52	(a)
	0	0.50	(b)
V_{Cd}·V_S	35	0.58−0.70	(a)
	50	0.59	(b)
	80	0.63−0.77	(a)
Hydrogenic donor	−253	0.03	(c)

[a]R. H. Bube and L. A. Barton, RCA Rev. **20**, 564 (1959).
[b]J. Woods, J. Electron. Control **5**, 417 (1958).
[c]H. H. Woodbury and M. Aven, Phys. Rev. B **9**, 5195 (1974).

$$(\epsilon/e)\frac{\partial}{\partial y}E(y,t)=[p(y,t)+p_t]-[n(y,t)+n_t]\ . \tag{3.3}$$

In Eqs. (3.1)—(3.3) the following definitions have been made: $n(y,t)$ $[p(y,t)]$ is the population of free photoexcited electrons (holes) (cm^{-3}); $G(y)$ $[R(y,t)]$ is the free carrier density generation (recombination) rate ($cm^{-3}s^{-1}$); $E(y,t)$ is the internal electric field due to the space charge accumulation ($V\,cm^{-1}$); μ_n (μ_p) is the free-electron (hole) mobility ($cm^2V^{-1}s^{-1}$); D_n (D_p) is the diffusion coefficient for free electrons (holes) (cm^2s^{-1}); ϵ is the dielectric constant of crystalline CdS ($=1.02$ pF/cm);[20] n_t (p_t) is the trapped electron (hole) population (cm^{-3}); and e is the elementary charge. The free carrier generation rate consists predominantly of carriers which will recombine nonradiatively, since radiative recombination occurs rapidly in time scales not interfering with carrier contributions to the photocurrent.[21] This leads[2] to the dependence of $G(y)$ on η_{nonrad},

$$G(y;\lambda)=\eta_{\text{nonrad}}\left[\frac{I_0\lambda}{hc}\right]\exp[-\beta(\lambda)y]\ , \tag{3.4}$$

where I_0 is the incident light irradiance ($W\,cm^{-2}$) at wavelength λ, and $\beta(\lambda)$ is the wavelength-dependent optical-absorption coefficient (cm^{-1}). The electron and hole recombination rate is given by the Shockley-Read statistics of the electron-hole pair nonradiative recombination through the mediation of a recombination center,[22]

$$R(y,t)=\frac{C_nC_p(np-n_1p_1)}{C_n(n+n_1)+C_p(p+p_1)}\ , \tag{3.5}$$

where $C_n(C_p)$ is the electron (hole) capture probability rate by the recombination center (s^{-1}); $n_1(p_1)$ is the equilibrium electron (hole) population (cm^{-3}), when $E_F=E_r$,

$$n_1p_1=n_i^2\ , \tag{3.6}$$

n_i is the intrinsic density of free carriers. For pure CdS crystals of high resistivity in the dark, the intrinsic and equilibrium free carrier densities are extremely small. Therefore, the following conditions are valid under optical excitation,

$$np\gg n_i^2\ , \tag{3.7a}$$

$$n\gg n_1\ , \tag{3.7b}$$

$$p\gg p_1\ . \tag{3.7c}$$

Eq. (3.5) can thus be simplified as

$$R(y,t)=\left[\frac{1}{C_pp(y,t)}+\frac{1}{C_nn(y,t)}\right]^{-1}\ . \tag{3.8}$$

The capture probability rates for electrons and holes depend on the location of the recombination centers in the semiconductor band gap. No such data for CdS are available to the authors' best knowledge, therefore, it was assumed for simplicity purposes that the recombination centers are located in a position such that $C_n=C_p\equiv C$, so that

$$R(y,t)=\frac{1}{\tau}\left[\frac{pn}{p+n}\right]\ , \tag{3.9}$$

where

$$\tau\equiv C^{-1} \tag{3.10}$$

is the lifetime of the free carriers. The electron and hole populations in the trapping states are related to those in the respective bands through Boltzmann factors,[23]

$$n_t=(N_t/N_c)n(y,t)\exp(E_{tn}/k_BT)\equiv X_nn(y,t) \tag{3.11}$$

and

$$p_t=(P_t/N_v)p(y,t)\exp(E_{t_p}/k_BT)\equiv X_pp(y,t)\ . \tag{3.12}$$

In Eqs. (3.11) and (3.12), N_t (P_t) is the electron (hole) trapping state density (cm^{-3}), N_c (N_v) is the effective density of states for electrons (holes) (cm^{-3}), and X_n (X_p) is defined as the electron (hole) trap factor. Substitution of Eqs. (3.11) and (3.12) into Poisson's Eq. (3.3) gives

$$(\epsilon/e)\frac{\partial}{\partial y}E(y,t)=(1+X_p)p(y,t)-(1+X_n)n(y,t)\ . \tag{3.13}$$

Equations (3.1), (3.2), and (3.13) contain three unknown quantities of interest, namely $n(y,t)$, $p(y,t)$, and $E(y,t)$. These equations can be solved numerically using a finite differences approach by dividing the thickness of the crystal into a number of thin sublayers as shown in Fig. 3. The finite difference forms of these equations can be written

$$\frac{n_i^{j+1}-n_i^j}{\Delta t}=G_i^j-R_i^j+\mu_n\left[\frac{n_i^{j+1}E_i^{j+1}-n_i^{j-1}E_i^{j-1}}{2\,\Delta j}\right]+D_n\left[\frac{n_i^{j+1}-2n_i^j+n_i^{j-1}}{(\Delta y)^2}\right]\ , \tag{3.14}$$

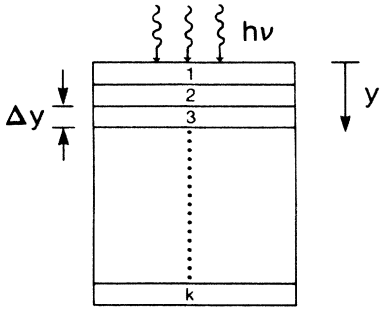

FIG. 3. Finite difference sublayering of photoexcited CdS single crystal.

$$\frac{p_i^{j+1}-p_i^j}{\Delta t}=G_i^j-R_i^j+\mu_p\left[\frac{p_i^{j+1}E_i^{j+1}-p_i^{j-1}E_i^{j-1}}{2\Delta y}\right]+D_p\left[\frac{p_i^{j+1}-2p_i^j+p_i^{j-1}}{(\Delta y)^2}\right], \tag{3.15}$$

and

$$\frac{E_i^{j+1}-E_i^{j-1}}{\Delta y}=\frac{e}{\epsilon}[(1+X_p)p_i^j-(1+X_n)n_i^j], \tag{3.16}$$

where the superscript (j) stands for position and the subscript (i) stands for time. To observe the compliance of Eqs. (3.14) and (3.15) with the physical requirement of charge neutrality within the bulk of the crystal, Eq. (3.14) can be written as follows:

$$\frac{n_i^{j+1}-n_i^j}{\Delta t}=G_i^j-R_i^j+\mu_n\left[\frac{(n_i^{j+1}E_i^{j+1}+n_i^jE_i^j)-(n_i^jE_i^j+n_i^{j-1}E_i^{j-1})}{2\Delta y}\right]+D_n\left[\frac{(n_i^{j+1}-n_i^j)-(n_i^j-n_i^{j-1})}{(\Delta y)^2}\right]. \tag{3.17}$$

Physically, the above equation is illustrated in Fig. 4(a). At the top and bottom surfaces of the crystal there is no carrier transport, as shown in Fig. 4(b). From Fig. 4 it is clear that, upon summing up all the drift terms,

$$\mu_n\left[\frac{n_i^2E_i^2+n_i^1E_i^1}{2\Delta y}\right]+\sum_{j=2}^{k-1}\mu_n\left[\frac{n_i^{j+1}E_i^{j+1}-n_i^{j-1}E_i^{j-1}}{2\Delta y}\right]-\mu_n\left[\frac{n_i^kE_i^k+n_i^{k-1}E_i^{k-1}}{2\Delta y}\right]=0, \tag{3.18}$$

and, upon summing up all the diffusion terms,

$$D_n\left[\frac{n_i^2-n_i^1}{(\Delta y)^2}\right]+\sum_{j=2}^{k-1}D_n\left[\frac{n_i^{j+1}-2n_i^j+n_i^{j-1}}{(\Delta y)^2}\right]-D_n\left[\frac{n_i^k-n_i^{k-1}}{(\Delta y)^2}\right]=0. \tag{3.19}$$

Equations (3.18) and (3.19) show that the drift and diffusion transport of carriers within the crystal is conserved. Further, summing up the individual sublayer contributions to the generation and recombination rates,

$$\sum_{j=1}^{k}\{[(G_i^j)_n-(G_i^j)_p]-[(R_i^j)_n-(R_i^j)_p]\}=0, \tag{3.20}$$

which shows charge conservation in the crystal.

Within the sublayer corresponding to the surface of the crystal, the carrier recombination rate increases due to the lattice discontinuity which introduces a larger defect density and conceivably larger impurity concentrations. The rate of carrier population recombination at the surface is given by[24]

$$R_s=\left[\frac{s}{\Delta h}\right]\frac{(p_sn_s-n_i^2)}{(n_s+n_i\exp[(E_r-E_i)/k_BT])+(p_s+n_i\exp[(E_i-E_r)/k_BT])}, \tag{3.21}$$

where n_s (p_s) is the electron (hole) density at the surface layer, s is the surface recombination velocity, and Δh is the thickness of the surface sublayer. For pure CdS crystals with high resistivity the following conditions hold at equilibrium:

$$p_sn_s \gg n_i^2, \tag{3.22a}$$

$$n_s \gg n_i\exp[(E_r-E_i)/k_BT], \tag{3.22b}$$

$$p_s \gg n_i\exp[(E_i-E_r)/k_BT]. \tag{3.22c}$$

In view of these conditions, Eq. (3.21) becomes

$$R_s\approx\left[\frac{s}{\Delta h}\right]\left[\frac{p_sn_s}{p_s+n_s}\right]. \tag{3.23}$$

B. Heat generation and diffusion formalism

After the carrier distributions have been determined, the heat generation processes within the crystal and the resulting temperature rise profiles in the solid and, through conduction, in the air can be calculated by the heat diffusion equations:[1]

$$\frac{\partial^2}{\partial y^2}\phi_s(y,t)=\frac{1}{\alpha_s}\frac{\partial}{\partial t}\phi_s(y,t)-\frac{\dot{Q}(y,t)}{k_s}, \tag{3.24}$$

for the crystal, and

$$\frac{\partial^2}{\partial y^2}\phi_g(y,t)=\frac{1}{\alpha_g}\frac{\partial}{\partial t}\phi_g(y,t), \tag{3.25}$$

for the gas, where $\phi_s(y,t)$ $[\phi_g(y,t)]$ is the temperature rise

in the crystal (air); α_s (α_g) is the thermal diffusivity of the crystal (air) ($cm^2 s^{-1}$); k_s is the thermal conductivity of the crystal ($W cm^{-1} deg^{-1}$); and $\dot{Q}(y,t)$ is the heat generation rate in the crystal ($W cm^{-2}$). The various mechanisms contributing to heat generation in a homogeneous semiconductor are,[2,25] (a) nonradiative thermalization of photoexcited electrons with energy greater than E_g; (b) heat production by bulk and surface nonradiative recombinations, which do not generate free carriers; (c) heat production by free carriers recombining nonradiatively; and (d) Joule heating in the presence of external applied electric fields due to photoexcited carrier acceleration. In Paper I of this work[18] it was found from a comparison between the PA and PC spectra of n-type CdS with and without an applied dc electric field, that the Joule effect was predominant in the sub-band-gap spectral range (i.e., around 520–540 nm) in the presence of fields on the order of 10 V or higher. Therefore, it was assumed in the present formalism that all other heat generation mechanisms are negligible in this range, compared to the generation rate due to the Joule effect,

$$\dot{Q}(y,t)=[\mu_n n(y,t)+\mu_p p(y,t)]eE^2 . \tag{3.26}$$

At the experimental optical modulation frequency of 20-Hz crystalline CdS is thermally thick.[1] This implies that thermal transfer at the crystal-backing interface can be neglected,

$$\frac{\partial}{\partial y}\phi_s \mid_{y=\text{back surface}}=0 . \tag{3.27}$$

At the upper surface of the crystal, which is exposed to the radiation, requirements for temperature and heat flux continuity across the solid-air interface yield the boundary conditions,

$$\phi_s(y=0,t)=\phi_g(y=0,t) , \tag{3.28}$$

$$k_s\frac{\partial}{\partial y}\phi_s(y=0,t)=k_g\frac{\partial}{\partial y}\phi_g(y=0,t) . \tag{3.29}$$

The boundary sublayer required for the solution of the heat diffusion equations in finite difference form at the crystal-air interface was defined in Fig. 5. The resulting set of finite difference equations can be written as follows:

$$\frac{\phi_{si}^{j+1}-2\phi_{si}^{j}+\phi_{si}^{j-1}}{(\Delta y)^2}=\frac{1}{\alpha_s}\left[\frac{\phi_{si+1}^{j}-\phi_{si}^{j}}{\Delta t}\right]-\frac{\dot{Q}(y,t)}{k_s} , \tag{3.30}$$

$$\frac{\phi_{g}^{j+1}-2\phi_{gi}^{j}+\phi_{gi}^{j-1}}{(\Delta y)^2}=\frac{1}{\alpha_g}\left[\frac{\phi_{gi+1}^{j}-\phi_{gi}^{j}}{\Delta t}\right] , \tag{3.31}$$

$$Q_i^j=[n_i^j\mu_n+p_i^j\mu_p]e(E_i^j)^2 , \tag{3.32}$$

$$\frac{\phi_{si}^{k+1}-\phi_{si}^{k-1}}{2\Delta y}=0 , \tag{3.33}$$

$$\phi_{si}^{1}=\phi_{gi}^{1} , \tag{3.34}$$

$$k_s\left[\frac{\phi_{si}^{0}-\phi_{si}^{2}}{2\Delta y}\right]=k_g\left[\frac{\phi_{gi}^{2}-\phi_{gi}^{0}}{2\Delta y}\right] , \tag{3.35}$$

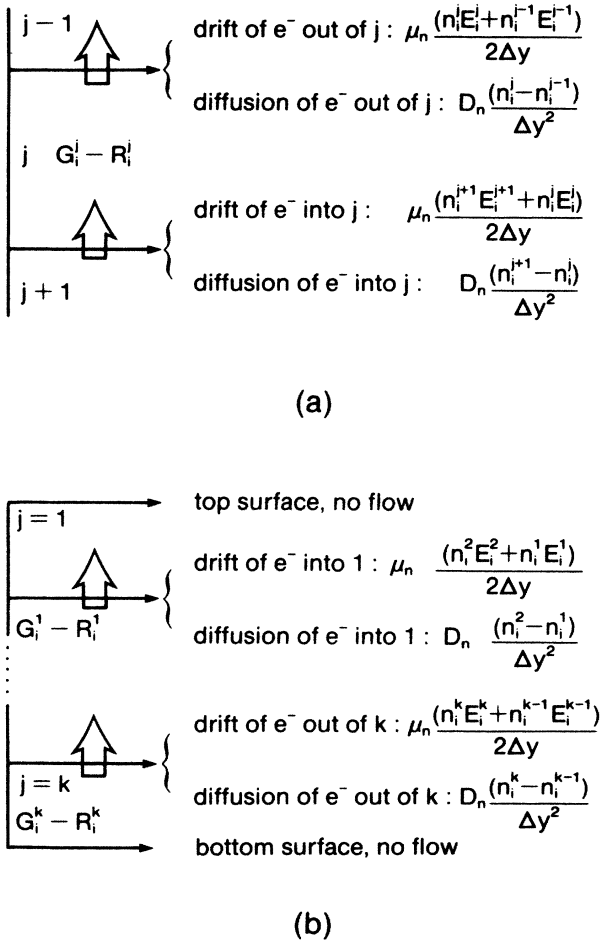

FIG. 4. Electron transport in finite difference crystal sublayers, including diffusion and drift term identifications. (a) bulk of the crystal; (b) surface layers.

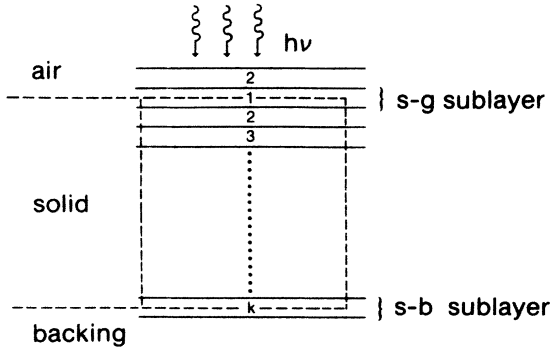

FIG. 5. Thermal diffusion in finite difference crystal sublayers showing the discretization of the upper and lower interfaces.

where, again, superscripts stand for position and subscripts stand for time. In order to determine the upper surface boundary condition, ϕ_{si}^0 in the artificial sublayer 1, Fig. 5, can be found from Eqs. (3.30) and (3.31) using $j=1$, eliminating the time increment term, and combining the result with Eq. (3.35):

$$\phi_{si}^0=\phi_{si}^2+(k_s/k_g)\left[2\phi_{gi}^2-\frac{(\Delta y)^2\dot{Q}(y,t)}{k_s}\right]. \tag{3.36}$$

Equations (3.30), (3.31), and (3.36) were used to determine the temperature profiles $\phi(y,t)$ in the crystal and in the air column above it. The PA cell pressure, which constitutes the photoacoustic signal, is given in the adiabatic ideal gas approximation by[1]

$$\Delta P(t)=(\gamma P_0/T_0)\langle\phi_g(t)\rangle_{\rm av}\ , \tag{3.37}$$

where P_0 and T_0 are the ambient pressure and temperature, γ is the ratio of the specific heats ($\gamma=1.4$ for air), and $\langle\phi_g(t)\rangle_{\rm av}$ is the space-averaged temperature rise in the air due to heat conduction from the solid.

C. Photocurrent formulation

The photocurrent is a function of the total number of free carriers that can reach the external circuit. The photoconductive behavior of photosensitive solids can be analyzed in terms of the decay range of the excess carriers,[26] i.e., the distance d through which photoexcited carriers drift under the action of an applied field before they are removed from the conduction or the valence band via recombination or capture events,

$$d_n=\mu_n\tau_nE,\quad d_p=\mu_p\tau_pE\ . \tag{3.38}$$

Data presented in Paper I[18] on sensitization and red quenching phenomena present in the secondary PA and PC spectra of CdS indicate that d_n and d_p are, in all likelihood, spectrally variant below the band gap, $d_n=d_n(\lambda)$ and $d_p=d_p(\lambda)$. Moss[27] introduced the photocurrent dependence on E_0, the maximum electric field magnitude required to drive all the free carriers to the electrodes:

$$I\propto E/E_0\ . \tag{3.39}$$

E_0 is inversely proportional to the decay range of free carriers. For our experiments[18] E_0 is expected to be wavelength dependent due to the sub-band-gap spectral variation of defect center densities at different photon energies in CdS.[9] Therefore,

$$E_0=E_0(\lambda)\equiv{\rm cf} \tag{3.40}$$

and the expression for the photocurrent density becomes

$$J(y,t;\lambda)=(eE/{\rm cf})[\mu_n n(y,t)+\mu_p p(y,t)] \tag{3.41}$$

where cf denotes the current density factor.[27]

IV. RESULTS AND DISCUSSION

The theoretical considerations of the preceding section were used to simulate the first cycle of the PA and PC responses of the CdS crystal with a transverse dc electric field, half a cycle under illumination, and the other half cycle in the dark. The PA response for each value of the absorption coefficient was determined by the peak pressure calculated in the air column above the sample. This peak response usually occurred in the second half of the cycle (dark). The phase lag was determined by the time delay between the half cycle point when the illumination ceased and the time when the pressure peak occurred. In the PC simulation the magnitude of the photocurrent was determined.

One important problem associated with the finite differences approach was the convergence of the solution. As the carrier transport equation is nonlinear, the maximum time step size for assured convergence cannot be determined theoretically. From preliminary simulation studies it was found that a time step size larger than 10 ns would induce oscillation and subsequent instability in the calculated carrier densities. The heat diffusion equations were more stable with respect to the time step size, provided that the latter satisfied the following criterion,[28]

$$\alpha_g\Delta t/(\Delta y)^2\le\tfrac{1}{2}\ . \tag{4.1}$$

Using $\Delta y=75$ μm and $\alpha_g=0.247$ cm^{2}s^{-1}, $(\Delta t)_{\rm max}$ was found to be 1.25×10^{-4} s for a stable solution to the heat diffusion equation, well above the required much finer time step for the transport equation stability. In the dark half cycle, the size of the time step was controlled so that the charge in carrier density due to recombination in any sublayers, Figs. 3 and 5, was less than one-half its original value. This empirical criterion was used to prevent the emergence of instabilities due to large carrier density fluctuation in each sublayer. In order to compromise computing time and accuracy, the thickness of the sublayers was set at 75 μm, corresponding to a spectral resolution up to $\beta\approx100$ cm^{-1}. In doing so, the accuracy in the short-wavelength band-gap and super-band-gap regions was compromised, but the general behavior of the PA and PC spectral responses was retained.

Table II shows the input data for pure n-type CdS. Widely varying surface recombination velocities have been reported for this material. The actual value of this parameter was shown not to affect the spectral shape of the PA and PC responses. Therefore the intermediate value of 10^4 cm/s was chosen for the purposes of this work. Nonradiative electron and hole recombination lifetimes of pure defect-rich CdS crystals depend very much on the defect density and surface preparation of a given crystal. The value $\tau_{\rm nonrad}\approx10$ μs given in Table II is a ceiling value on a number of measurements using pulsed laser deexcitation studies of CdS under various excitation power levels using a nitrogen pumped dye laser. (Ref. 3, Table II). Lifetime values as high as tens of milliseconds have been quoted elsewhere.[2,29] The spectral shape of the PA and PC responses *is affected* by the absolute value of $\tau_{\rm nonrad}$ chosen for a given CdS crystal. The value $\tau_{\rm nonrad}$ ultimately used can be deduced, in principle, from a fitting of the theoretical responses to the experimental PA and PC spectra. The values for X_n and X_p in Table II have been determined using Eqs. (3.11) and (3.12) and the effective densities of states

$$N_c=2(2\pi m_e^*k_BT/h^2)^{3/2}\ , \tag{4.2}$$

$$N_v = 2(2\pi m_h^* k_B T/h^2)^{3/2} . \quad (4.3)$$

The trapping state ionization energies E_{tn} and E_{tp} were assumed to be those responsible for the 0.24-eV V_s^{2-} vacancy level below the conduction band edge, and the 0.29-eV unknown species acceptor level above the filled band, respectively, in Fig. 1. The trapping state densities were altogether unknown and were used as adjustable parameters. The phenomena of sub-band-band sensitization and red quenching,[18] which are consequences of trap level

TABLE II. (a) Pure CdS input data for PA and PC theoretical simulation. (b) Physical properties of CdS single crystals as a function of absorption coefficient.

(a)

Environmental Conditions
Ambient Temperature: 280 K
Ambient Pressure: 101.3 kPa

Simulation Conditions
Incident light intensity: 10^{-4} W/cm
Magnitude of ext. electric field: 10 V/cm
Modulation frequency of incident radiation: 20 Hz
Crystal thickness: 0.15 cm
Thickness of the air column: 0.15 cm
Thickness of each sublayer: 75 μm

Physical Properties of Air
Thermal Conductivity:[a] 2.6×10^{-4} J/cm °C
Thermal Diffusivity:[a] 0.247 cm^2/s
Ratio of specific heats:[a] 1.4

Input Physical Properties of CdS Single Crystals
Thermal Conductivity:[b] 0.272 J/cm °C
Thermal Diffusivity:[b] 0.153 cm^2/s
Average lifetime of free carriers:[c] 10^{-5} s
Mobility of electron/hole:[d] 350/50 cm^2/V s
Diffusion coefficient of electron/hole:[e] 9.0/1.3 cm^2/s
Average surface recombination velocity:[b,f] 10^4 cm/s

(b)

β (cm^{-1})	λ(nm)[g,h]	X_n[i]	X_p[j]	cf[k]
100.0	518.0	0.50	0.50	60
80.0	518.5	0.48	0.50	57
70.0	519.0	0.46	0.50	54
60.0	520.0	0.44	0.50	51
50.0	521.0	0.42	0.50	48
40.0	522.0	0.40	0.50	45
30.0	523.0	0.38	0.50	42
20.0	524.0	0.36	0.50	39
10.0	525.0	0.34	0.50	36
8.0	526.0	0.32	0.50	33
7.0	527.0	0.30	0.50	30
6.0	528.0	0.28	0.50	27
5.0	529.0	0.26	0.50	24
4.0	530.0	0.24	0.50	21
3.0	531.0	0.22	0.50	18

[a]A. Rosencwaig, in *Photoacoustics and Photoacoustic Spectroscopy* (Wiley, New York, 1980), p. 96.
[b]Reference 2.
[c]J. H. Richardson, S. P. Perone, and S. B. Deutscher, J. Phys. Chem. **85**, 341 (1981).
[d]J. L. Boone and G. Cantwell, J. Appl. Phys. **57**, 1171 (1985).
[e]Einstein's relation.
[f]D. Huppert and M. Evenor, J. Vac. Sci. Technol. **A2**, 532 (1984).
[g]D. Dutton, Phys. Rev. **112**, 785 (1958).
[h]D. G. Thomas, J. J. Hopfield, and M. Power, Phys. Rev. **119**, 570 (1960).
[i]Equation (3.11).
[j]Equation (3.12).
[k]Equation (3.40).

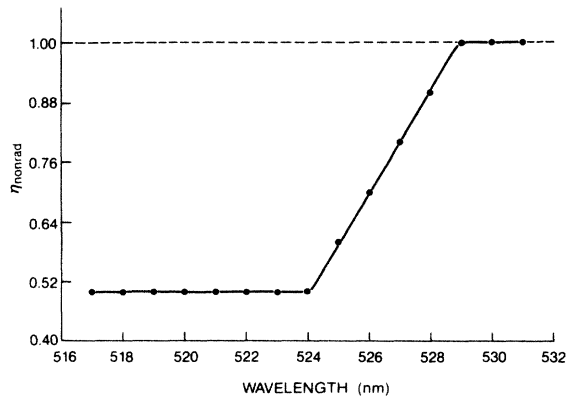

FIG. 6. Calculated spectral variation of the nonradiative quantum efficiency for best fit to the data of Ref. 18, Fig. 5.

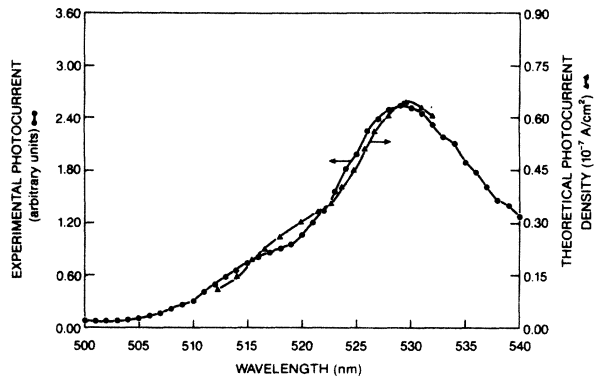

FIG. 8. Experimental (—●—●—) and theoretical (—▲—▲—) PC magnitude of pure CdS with a transverse electric field of 10 V dc. Light modulation frequency: 20 Hz; spectral resolution: 2 nm. Theoretical sublayer thickness: 75 μm; $\tau_{nonrad}=10^{-5}$ s.

filling with photoexcited carriers were accounted for by assuming that the electron trap density factor X_n decreases monotonically from the short wavelength end to the long-wavelength tail of the PA and PC spectra. Hole trapping, however, was assumed to remain constant throughout the CdS spectrum, since infrared (ir) photons would be required to induce the valence band-to-E_{tp} level transitions. The E_{tp} level, Fig. 2, is thus assumed to be contributing to the photocurrent solely as a result of thermal excitations and will not be expected to play a spectral shaping role in the recombination process.[30]

The photocurrent density is inversely proportional to E_0, Eq. (3.41). E_0 depends on the electron and hole mobilities, as well as on the crystal defect densities which govern trapping and free carrier scattering mechanisms.[31] Consistency with the spectral dependence of the trap density factor X_n required that trapping and scattering mechanisms should become less important with increasing wavelength of the exciting radiation, as the direct result of decreased available trap densities in the sub-band-gap region. Therefore, $E_0(\lambda)$ was assumed to decrease monotonically in Table II, with the maximum value of 60 V/cm chosen so as to yield the best fit between the theoretical and experimental[18] PC response curves.

To the best of the authors' knowledge, no systematic study of the possibility of any spectral dependence of the nonradiative quantum efficiency of pure CdS crystals has been carried out previously. Bandeira *et al.*[2] assumed no such dependence for their sample, however, this assumption was suggested[18] to be qualitatively inconsistent with nonradiative phenomena observed by many workers at sub-band-gap wavelengths. Richardson *et al.* (Ref. 3, Table II) have reported rapidly increasing quantum yields (electron flow per incident photon) for wavelengths longer than the bandedge of CdS. The problem of unknown values for any wavelength dependence of η_{nonrad} in the present work was overcome by assuming a general functional dependence,

$$\eta_{nonrad}=\eta_{nonrad}(\lambda) \tag{4.4}$$

and computationally optimizing Eq. (4.4) for best agreement with experimental PA and PC spectroscopic data. The functional relationship shown in Fig. 6 was found to yield the best correspondence between the theoretical and the experimental (paper I, Fig. 5) combined PA and PC spectra. This correspondence is shown in Figs. 7–9. The

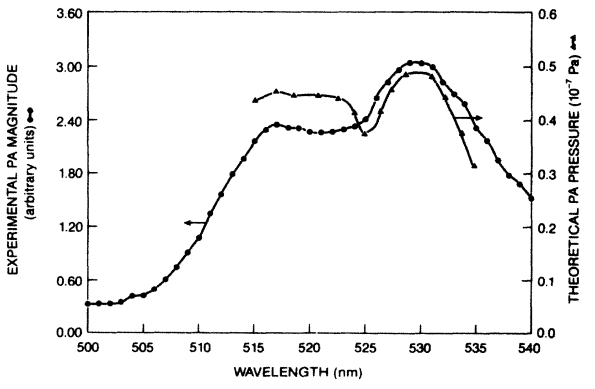

FIG. 7. Experimental (—●—●—) and theoretical (—▲—▲—) PA magnitude of pure CdS with a transverse electric field of 10 V dc. Light modulation frequency: 20 Hz; spectral resolution: 2 nm. Theoretical sublayer thickness: 75 μm; $\tau_{nonrad}=10^{-5}$ s.

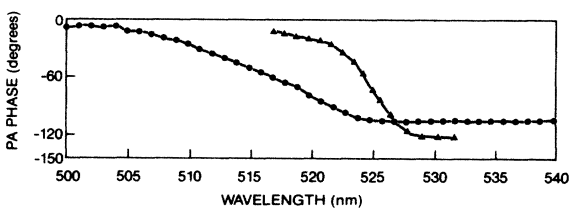

FIG. 9. Experimental (—●—●—) and theoretical (—▲—▲—) PA phase lag corresponding to spectrum in Fig. 7.

theoretical PA magnitude exhibits two maxima at approximately 520 and 529 nm. The theoretical PC magnitude exhibits a shoulder at approximately 518 nm and a maximum at approximately 530 nm. Figures 7 and 8 indicate a generally good agreement between theory and experiment. The apparent red shift of the theoretical PA and PC magnitudes corresponding to the high-energy peak and shoulder, respectively, is mainly due to the limitations of the spatial sublayer finite thickness in the computational simulation ($\Delta y = 75$ μm): The relatively thick surface depletion layer used in the present model caused the theoretical transition from surface to bulk absorption to be shifted to the long-wavelength region. The 530-nm maximum, however, was not affected by the size of the sublayer thickness, because (i) it lies in a transparent spectral region (bulk absorption); and (ii) its position is governed by the nonradiative quantum efficiency profile and not by the carrier distribution in the crystal.

The theoretical PA phase lag of Fig. 9 shows trends similar to the measured phase. It exhibits a small lag in the high-absorption region due to the onset of photoacoustic saturation. The total phase lag over the entire spectral region of the simulation (517—530 nm) is, however, larger than the experimental phase. In terms of our models' limitations, a possible reason for this discrepancy is that $\Delta y = 75$ μm tends to distribute free carriers more evenly inside the crystal bulk than thinner sublayers would, with the result of long diffusive time lags. This effect was verified computationally with Δy as a parameter (see Table III). Phenomenologically, some discrepancies between theory and experiment in Figs. 7—9 may be accounted for by the fact that the nonradiative lifetime was taken to be independent of wavelength although there is evidence[32] that it decreases in going from long wavelengths toward the band gap. Such decreases would tend to lower the PA phase lag, which has been verified computationally with the carrier lifetime as a parameter (see Table III). They would also tend to shift the bulk crystal heat centroid toward the surface, thus producing a stronger PA signal in the sub-band-gap wavelengths. This effect would increase the 529-nm peak to 517-nm peak size ratio in Fig. 7, in closer correspondence with the experimental PA spectrum shown in that figure.

Table III lists a summary of the major theoretical cause-effect relationships between the PA and PC responses and various important carrier transport parameters in pure CdS crystals. That table was assembled using the theory developed in this work. The most important conclusion from Table III is that *only* a wavelength variation of $\eta_{\text{nonrad}} = \eta_{\text{nonrad}}(\lambda)$ such as shown in Fig. 6 is capable of generating the experimentally observed PA and PC peaks at about 530 nm. Numerical spectra obtained with

TABLE III. Summary of the cause-effect relationships between CdS crystal parameters and photoacoustic and photocurrent response.

Parameter variation in	Effect on the theoretical PA and PC spectra	
	Photoacoustic	Photocurrent
Lifetime, $\tau(\lambda)$	Induce vertical shift Shift high energy maximum Vary phase shift	Induce vertical shift
Sublayer thickness (limited by computation time requirements)	Induce vertical shift Shift high energy maximum Vary magnitude of first maximum Vary phase shift	Induce vertical shift
$\eta_{\text{nonrad}}(\lambda)$	Responsible for the production of the low energy maximum No change in the phase shift	Responsible for the production of the 529 nm maximum
Trap density factor, $X_n(\lambda)$	Induce vertical shift or minor relative spectral shift of the two maxima depending on input trap density factor	Induce vertical shift
Current factor, $E_0(\lambda)$	No change in magnitude or phase	Induce vertical shift or disappearance of high energy shoulder, depending on input data
Surface recombination velocity	Induce shift in the high absorption end signal magnitude Induce slight phase shift	Induce slight shift in high absorption end signal magnitude

η_{nonrad}=constant generated a high-energy peak at around 523 nm only, with no evidence of a second peak. Table III further shows that the appearance of the high-energy PA spectral peak and PC shoulder is consistent with intrinsic band-to-band recombinations. Its magnitude and spectral position can be controlled by intrinsic transition properties (i.e., recombination lifetime), numerical resolution (Δy) and surface recombination velocity.

At this time there has been no other functional quantitative relation, such as Eq. (4.4) and Fig. 6 reported in the literature for CdS or, indeed, any other semiconductors. Kitamura *et al.*[33] have recently studied nonradiative recombination processes in Ge-doped As_2Se_3 chalcogenide glasses using microphone gas-coupled PAS. Glasses of the type $(As_2Se_3)_{1-x}Ge_x$, although noncrystalline, exhibit optical-absorption gaps[34] with substantial subgap PA contributions due to the high-defect densities present in that optical region. Using direct comparison between the PA and optical-absorption spectra and finite electron-phonon coupling probabilities, these authors showed the chalcogenide glasses exhibited rapid increases in nonradiative quantum efficiencies at subgap energies, similar to the functional form of Fig. 6 in CdS. $\eta_{\text{nonrad}}(\lambda)$ increases ranged between approximately 35% and 80%, depending on the mole fraction x. This analogy may be well substantiated, in view of the large native defect densities present in our particular n-type CdS crystals[18] in the sub-band-gap region. Figure 6 shows that η_{nonrad} can be taken to be independent of λ in the super-band-gap region $\lambda \leq 524$ nm. Therefore, it is expected that in this spectral range the theory of Bandeira *et al.*[2] will be valid and will constitute the proper limit of the generalized theory presented in this work. Our identification of the high-energy PA peak in Fig. 7 as due to the intrinsic excitation is thus in agreement with the single PA peak assignation by those authors around 521 nm.

V. CONCLUSIONS

The finite differences theoretical model of the combined PA and PC responses of high resistivity n-type CdS single crystal showed that major experimental results from Paper I can be explained by two spectrally resolved mechanisms: (i) band-to-band recombinations in the band-gap region (517–522 nm), and (ii) the spectral variation of $\eta_{\text{nonrad}}(\lambda)$ between approximately 524 and 530 nm. The latter effect is consistent with large native defect densities at sub-band-gap wavelengths and can be used to characterize the degree of perfection of specific CdS crystals. The theory presented in this work requires optical-absorption coefficient data inputs and optimization of electronic parameters through best fits to PA and PC spectra. Its efficiency can be limited by computing time and/or computer speed limitations, especially in the super-band-gap spectral region, however, for most cases a Digital Equipment Corporation PDP-11/23 computing facility will suffice. Otherwise, the theory is quite general and can be used with other semiconductors besides CdS.

ACKNOWLEDGMENT

The authors wish to acknowledge the financial support of the Natural Sciences and Engineering Research Council (NSERC) of Canada throughout the work accomplished in both parts of this report.

[1]A. Rosencwaig and A. Gersho, J. Appl. Phys. **47**, 64 (1976).
[2]I. N. Bandeira, H. Closs, and C. C. Ghizoni, J. Photoacoust. **1**, 275 (1982).
[3]L. C. M. Miranda, Appl. Opt. **21**, 2923 (1982).
[4]V. A. Sablikov and V. B. Sandomirskii, Fiz. Tekh. Poluprovodn. **17**, 81 (1983) [Sov. Phys.—Semiconductors **17**, 50 (1983)]; and V. A. Sablikov and V. B. Sandomirskii, Phys. Status Solidi B **120**, 471 (1983).
[5]A. N. Vasil'ev and V. B. Sandormirskii, Fiz. Tekh. Poluprovodn. **18**, 1751 (1984) [Sov. Phys.—Semiconductors **18**, 1095 (1984)].
[6]A. N. Vasil'ev and V. B. Sandormirksii, Fiz. Tekh. Poluprovodn. **18**, 1954 (1984) [Sov. Phys.—Semiconductors **18**, 1221 (1984)].
[7]A. Mandelis, Chem. Phys. **81**, 185 (1983).
[8]R. S. Quimby and W. M. Yen, J. Appl. Phys. **51**, 4985 (1980).
[9]R. H. Bube, J. Chem. Phys. **23**, 18 (1955).
[10]I. Uchida, J. Phys. Soc. Jpn. **22**, 770 (1967).
[11]P. Mark, Phys. Rev. **137**, A203 (1965).
[12]W. van Roosbroeck, Phys. Rev. **119**, 636 (1960).
[13]M. A. Rizakhanov, Yu N. Emirnov, F. S. Gabibov, M. M. Khamidov, and M. K. Sheinkman, Fiz. Tekh. Poluprovodn. **12**, 1342 (1978).
[14]N. Susa, H. Watanabe, and M. Wada, Jpn. J. Appl. Phys. **15**, 2365 (1976).
[15]M. R. Brown, A. F. J. Cox, W. A. Shand, and J. M. Williams, J. Lumin. **3**, 96 (1970).
[16]K. Mochizuki, M. Satoh, and K. Igaki, Jpn. J. Appl. Phys. **22**, 1414 (1983).
[17]H. Wada. H. Yoshioka, J. Morimoto and T. Miyakawa, Jpn. J. Appl. Phys. **24**, Suppl. 24-1, 1217 (1985).
[18]A. Mandelis and E. K. M. Siu, preceding paper, Phys. Rev. B **34**, 7209 (1986).
[19]R. H. Bube, J. Phys. Chem. **1**, 234 (1957).
[20]R. H. Bube, RCA Rev. **20**, 565 (1959).
[21]R. H. Bube, *Photoconductivity of Solids* (Wiley, New York, 1960), p. 391.
[22]W. Shockley and W. T. Read, Jr., Phys. Rev. **87**, 5 (1952).
[23]A. Rose, *Concepts in Photoconductivity and Allied Problems* (Wiley, New York, 1978), p. 19.
[24]A. S. Grove, *Physics and Technology of Semiconductor Devices* (Wiley, New York, 1967), p. 138.
[25]W. Thielemann and B. Rheinländer, Solid-State Electron. **28**, 1111 (1985).
[26]F. Stockmann, Z. Physik **138**, 404 (1954).
[27]T. S. Moss, *Photoconductivity in the Elements* (Academic, New York, 1953), p. 25.
[28]C. F. Gerald, *Applied Numerical Analysis* (Addison-Wesley, New York, 1980), p. 395.
[29]Z. Harzion, D. Huppert, S. Gottesfeld, and N. Croitoru, J. Elecroanal. Chem. **150**, 571 (1983).
[30]R. H. Bube, Proceedings IRE **43**, 1836 (1955).

[31]R. A. Smith, *Semiconductors* (Cambridge University Press, Cambridge, 1959), p. 148.
[32]J. Lambe, Phys. Rev. **98**, 985 (1955).
[33]M. Kitamura, T. Ogawa, and T. Arai, J. Phys. Soc. Jpn. **52**, 2561 (1983).
[34]N. F. Mott and E. A. Davis, *Electronic Processes in Non-Crystalline Materials* (Clarendon, Oxford, 1979), p. 43.